ELSEVIER

J. Non-Newtonian Fluid Mech. 97 (2001) 99–124

Journal of Non-Newtonian Fluid Mechanics

www.elsevier.com/locate/jnnfm

On the reproducibility of the rheology of shear-thinning liquids

M.P. Escudier [a,*], I.W. Gouldson [a], A.S. Pereira [b], F.T. Pinho [c], R.J. Poole [a]

[a] *Department of Engineering, Mechanical Engineering, University of Liverpool, Liverpool L69 3GH, UK*
[b] *Instituto Superior de Engenharia do Porto, Rua de São Tomé, 4100 Porto, Portugal*
[c] *Centro de Estudos de Fenómenos de Transporte DEMEGI, Faculdade de Engenharia, Universidade do Porto, Rua dos Roberto Frias, 4200-465, 4050-123 Porto, Portugal*

Received 26 March 1998; received in revised form 19 September 2000

Abstract

The independent analysis of flow measurements is frequently hampered by incomplete characterisation of the working fluid. This problem is particularly acute in situations which require working fluids with identical properties, such as the development of scaling laws for the turbulent flow of drag-reducing liquids. In this paper, we demonstrate that the viscometric viscosity, loss and storage moduli for two of the most common polymers used for flow experiments, carboxymethylcellulose (CMC) and xanthan gum (XG), are practically insensitive to the chemistry of the tap water used as a solvent, to the method of mixing, and to the biocide added. However, the properties of CMC from two different manufacturers were found to be significantly different, whereas there was no difference between XG solutions prepared from different batches from the same manufacturer. Our conclusion is that for a given concentration in water, the properties of certain non-Newtonian liquids, such as CMC and XG, are essentially fixed and reproducible. Although the situation is less than ideal, comparisons of fluid-flow data from entirely independent laboratories can thus be made even in the absence of direct rheological measurements.

Keywords: Carboxymethylcellulose; Xanthan gum; Viscosity; Loss and storage moduli; Reproducibility

1. Introduction

Scaling of data for the turbulent flow of drag-reducing non-Newtonian liquids remains an unsolved problem of great practical significance. In the absence of theoretical guidance, reliance has to be placed on experiments carried out with identical fluids in geometrically similar configurations at appreciably different scales. Few individual laboratories have the resources to carry out such parallel experiments and ideally a coordinated collaborative effort between several laboratories is required. Unfortunately, such collaborations are few and far between and attempts to analyse published data are often hampered because

* Corresponding author. Fax: +44-151-794-4848.
E-mail address: escudier@liv.ac.uk (M.P. Escudier).

0377-0257/01/$ – see front matter
PII: S0377-0257(00)00178-6

Nomenclature

a	parameter in Carreau–Yasuda model
B	bias limit
G'	storage modulus (Pa)
G''	loss modulus (Pa)
L	cylinder length (m)
m	power-law exponent for Cross model
M	torque (N m)
n	power-law exponent for Carreau–Yasuda model
N	number of data points in sample
P	precision limit
r_{I}	inner radius of inner gap (m)
r_{O}	inner radius of outer gap (m)
R	Pearson correlation coefficient
R_{I}	outer radius of inner gap (m)
R_{O}	outer radius of outer gap (m)
t	time (s)
U	uncertainty

Greek letters

$\dot{\gamma}$	shear rate (s^{-1})
$\dot{\gamma}_{\mathrm{MAX}}$	maximum shear rate (s^{-1})
$\dot{\gamma}_{\mathrm{MIN}}$	minimum shear rate (s^{-1})
ε	radius ratio
θ	sensitivity coefficient
λ_{CR}	time constant in Cross model (s)
λ_{CY}	time constant in Carreau–Yasuda model (s)
μ	apparent viscosity $\tau/\dot{\gamma}$ (Pa s)
μ_{CR}	value of μ calculated from Cross model (Pa s)
μ_{CY}	value of μ calculated from Carreau–Yasuda model (Pa s)
μ_{M}	value of μ derived from measurements (Pa s)
μ_{MAX}	maximum μ_{M} (Pa s)
μ_{MIN}	minimum μ_{M} (Pa s)
μ_0	asymptotic value of μ for zero shear rate (Pa s)
μ_∞	asymptotic value of μ for infinite shear rate (Pa s)
σ_{A}	standard deviation between μ_{M} and reference μ_{CY}
σ_{I}	inherent standard deviation between μ_{M} and μ_{CY}
τ	shear stress (Pa)
τ_{MAX}	maximum shear stress (Pa)
τ_{MIN}	minimum shear stress (Pa)
ω	angular velocity (rad/s)

characterisation of the working fluid is inadequate, often limited to the concentration of a polymer in water and a power-law representation of the flow curve. By increasing the number of free parameters in the viscosity model, the fit to measured data can be improved but there will still be an inherent deviation due to inaccuracies in the model, scatter in the data and other systematic uncertainties in the measurement of the flow curve. What is still ignored, however, are the possible influences on the fluid rheology of such factors as the solvent chemistry, especially pH and salinity, the mixing procedure, and differences in the polymer chemistry. Hoyt [1], for example, was limited to the data of Ollis [2], De Loof et al. [3] and Wang [4] with which to test his negative roughness scaling hypothesis for pipe flow. Similarly, the incomplete fluid characterisations of Allan et al. [5] and Luchik and Tiederman [6] prevents comparisons with the results for the nominally identical polyacrylamide solutions of Hartnett [7], who clearly demonstrated that changes in the solvent chemistry can affect the viscosity of a given solution by as much as one order of magnitude. Our own experience with carbopol is similar, with major variations being found in the properties of nominally identical solutions. Another good example of this lack of consistency is associated with the work of Reischman and Tiederman [8]. Although initially reported to have a constant viscosity, Tiederman et al. [9] subsequently indicated that the viscosity of their fluid was in fact variable, a result confirmed by the data of Hartnett [7]. On the other hand, Escudier et al. [10] were able to demonstrate that Hoyt's [1] negative roughness concept provided a basis for scaling the results of data for the turbulent flow of 0.2% carboxymethylcellulose through a concentric annulus using both their own data and those for a smaller scale experiment reported by Nouri et al. [11] even though the latter provided only a power-law representation of the flow curve for a different brand of CMC.

In the present paper, we report on the experience of two research groups, one in Liverpool the other in Porto, which have been carrying out experiments on the turbulent flow of shear-thinning polymer solutions (tylose, carboxymethylcellulose (CMC), xanthan gum (XG) and polyacrylamide) through pipes, annuli and sudden expansions at different scales (typically 2:1). To minimise and quantify uncertainties associated with the fluid rheology in comparing our results, we have quantitatively analysed the errors in our characterisation procedures, established whether our solvents (local tap water), biocides and preparation procedures affect fluid rheology, and identified the extent to which the polymers themselves differ. So far as we are aware, this is the first time in which two separate groups have attempted to standardise the preparation and characterisation of non-Newtonian liquids in common use in turbulent-flow experiments. Such an approach is essential at a time when strenuous efforts are being made to relate hydrodynamic and heat transfer behaviour to the rheological properties of non-Newtonian liquids. The advantage of such a standardised approach has been recognised in the past by rheologists and progress made towards some common ground for carefully formulated oil-based viscoelastic liquids of high viscosity, as in the M1 and Al fluid experiments reported by JNNFM [12] and Hudson and Jones [13], respectively.

2. Measuring programme and fluid preparation

For the present work, moderately high concentrations of the two polymers most commonly used by the Liverpool and Porto research groups (0.4% CMC and 0.25% XG) were chosen to achieve relatively high levels of both viscosity and viscoelasticity in order to improve the accuracy of the measurements. The CMC solutions were used to investigate the influence of similar polymer additives from two different manufacturers, i.e. similar brand names and grades, whereas the XG solutions are used to investigate the effects of biocide and method of mixing. The CMC used by the Liverpool group has a molecular weight of

Table 1
Chemical analysis of the solvent (tap water)

	Porto	Liverpool
pH	6.9	7.6
Alkalinity (mg/l of HCO_3)	65.9	29
Chlorides (mg/l)	11.9	24.8
Nitrates (mg/l)	6.2	7.05
Sulphates (mg/l)	31.0	33.8
Calcium (mg/l)	21.4	18.9
Magnesium (mg/l)	4.96	2.87
Iron (mg/l)	0.05	0.0705

about 700 000 kg/kg mol and was supplied by Aldrich Chemical Co. whilst that in Porto was manufactured by Hercules (grade 7H4C, molecular weight about 300 000 kg/kg mol). The XG was nominally the same in Liverpool and Porto, Keltrol TF from Kelco with a molecular weight in excess of 10^6 kg/kg mol, although undoubtedly from different manufacturing batches since they were purchased separated by more than a 2 year time gap.

For each polymer, solutions were mixed using both Liverpool and Porto tap water. A four-letter code (ABCD) is used to identify each fluid with A identifying the origin of the polymer (L for Liverpool, P for Porto), B the origin of the water and place of mixing (again L or P), C the polymer (X for XG, C for CMC) and D the biocide: 0.02% Kathon LXE from Rohm and Haas (K) or 100 ppm formaldehyde (F), the biocides normally used in Porto and Liverpool, respectively.

The chemical composition of the Porto tap water was analysed at the Department of Chemical Engineering at the University of Porto and that of the Liverpool tap water was provided by the drinking water register of the supplier, North West Water Limited in Liverpool. The results are presented in Table 1.

In Porto the polymer in powder form was added to 4 kg of non-filtered tap water with 200 ppm of the biocide Kathon. As the polymer was being added to the water in a 10 l covered vessel, the solution was agitated by a four-bladed pitched impeller, powered by an 18 W motor rotating at 700 rpm. After adding all the polymer, the rotational speed was reduced to 200 rpm and the agitation continued for a further 90 min, which was sufficient to completely dissolve the polymer. At the end of this operation any water condensed on the inside surface of the tank lid was returned to the mixture and the solution agitated for 5 min, with the stirred vessel again closed by the lid. The solution was then left standing for 24 h to completely hydrate the molecules prior to shipment to Liverpool where all rheological measurements were carried out. The shipments were delivered within 54 h of preparation. The solution was again agitated for 30 s in order to fully homogenise it immediately before making the measurements.

In Liverpool polymer was added to 3 kg of non-filtered tap water contained in a 5 l vessel. A four blade impeller was used to mix the fluid at the maximum rotational speed obtainable without entraining air (560–1000 rpm) until it was visibly homogeneous. 24 h was allowed for the mixture to hydrate and the fluid agitated prior to testing to ensure homogeneity.

It should be noted that for our hydrodynamic work (reported elsewhere) the polymer solutions are prepared differently in Porto and Liverpool. In Porto, the procedure is similar to that described above, except that either a 100 or 400 l tank is used, according to the amount of fluid required by the particular experimental rig to be used (see Pereira and Pinho [14] and Coelho et al. [15]). In Liverpool, the solutions

are mixed in one of two 800 l mixing loops, such as the annular flow rig described by Escudier et al. [10]. In this case, the polymer is added to a large tank while the solution is circulated through a mixing loop, by a Mono pump for a period of 10 h, after which it is left standing for 30 h to hydrate the molecules. Prior to taking samples for the rheometer the fluid is mixed for at least 30 min to homogenize it. No significant differences were found when the results obtained here with solutions prepared in the small stirred vessels were compared with the data for the same fluids prepared in the flow loops in Liverpool and in the large stirred vessels in Porto.

3. Measuring equipment and uncertainties

All measurements were carried out in Liverpool using a TA Instruments Rheolyst AR 1000N controlled-stress rheometer. A 4 cm diameter parallel plate geometry was used to achieve the highest possible shear rates (10^3–$2 \times 10^4\ s^{-1}$). For a wide range of intermediate shear rates (10^{-2}–$10^3\ s^{-1}$) a 6 cm diameter 2° acrylic cone was used. The lowest shear rates were achieved using a 4.12 cm mean diameter double concentric cylinder arrangement, in steady shear down to shear rates close to $10^{-3}\ s^{-1}$ and using the creep mode to extend the range to $5 \times 10^{-4}\ s^{-1}$. Creep data were also obtained at higher shear rates to confirm the validity of the procedure. All measurements were carried out at a temperature of 20°C. Temperature control of the TA rheometer is achieved via a plate that uses the Peltier effect to control the temperature of the sample within ±0.1°C. The instrument is capable of performing measurements of the viscometric viscosity in steady shear flow and of the complex dynamic viscosity in oscillatory shear flow. Although the rheometer is in principle capable of measuring the first normal stress difference, for the two polymer solutions investigated here the magnitude of this property is below the sensitivity of the instrument for concentrations below about 1%. The paper is limited therefore to measurements of the flow curve and the loss and storage moduli. A detailed uncertainty analysis, which was performed for the double-concentric gap geometry, is presented in Appendix A. The final outcome is that for $\dot{\gamma} > 1\ s^{-1}$ the total uncertainty is about 2%. For the cone-and-plate and parallel-plate geometries at high shear rates, the same values of total uncertainty apply because in that range the uncertainty is dominated by the angular speed contribution which is independent of the geometry used.

4. Results and discussion

4.1. Viscometric viscosity

4.1.1. Xanthan gum (XG)

The overall consistency of the XG viscosity data over almost eight decades of shear rate is evident from Fig. 1. Also included in Fig. 1 is a curve representing the Carreau–Yasuda model [16]:

$$\mu_{CY} = \mu_\infty + (\mu_0 - \mu_\infty)[1 + (\lambda_{CY}\dot{\gamma})^a]^{n/a}, \tag{1}$$

μ_0 being the zero-shear-rate viscosity, μ_∞ the infinite-shear-rate viscosity, λ_{CY} a time constant, n a power-law index and a a parameter introduced by Yasuda et al. [16] to describe the transition region between the zero-shear-rate and power-law regions. In principle, there are several different methods by

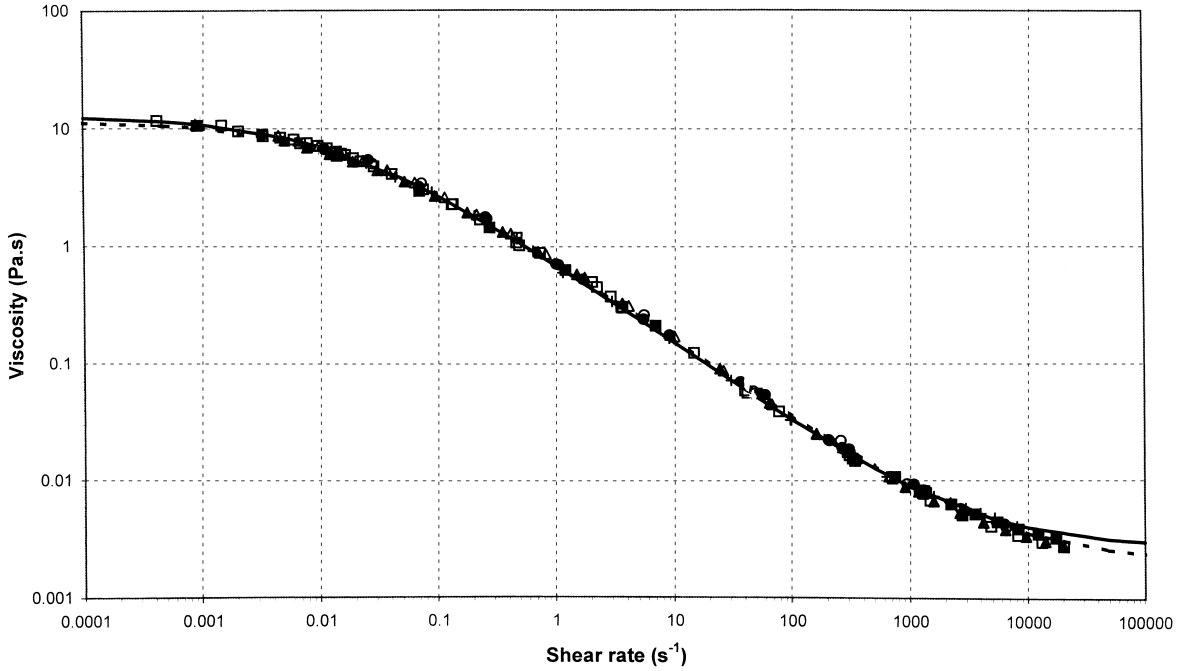

Fig. 1. Viscometric viscosity of xanthan gum solutions together with Carreau–Yasuda (—) and Cross (– – – –) model fits: (□) LLXF; (●) LLXF2; (○) LLXF3; (■) LPXF; (△) PLXF; (▲) PPXF; (+) PPXK.

which to determine the model parameters μ_0, μ_∞, λ_{CY}, n and a. For example, minimisation of one of either of the following standard deviations could be used

$$\sum_N (\mu_M - \mu_{CY})^2 \text{ or } \sum_N (1 - \mu_M/\mu_{CY})^2, \tag{2}$$

where μ_M is the measured apparent viscosity (i.e. $\tau/\dot{\gamma}$) at a particular shear rate, and μ_{CY} the value of the viscosity calculated from the Carreau–Yasuda model at the same shear rate, and N the number of data points. In our view, the latter is to be preferred because for fluids where (as here) the range of μ_M covers several orders of magnitude, the former quantity is heavily weighted (for shear-thinning liquids) towards the low shear-rate data. The Carreau–Yasuda model is a better representation of XG viscosity at low shear rates than the Carreau model ($a = 2$ in Eq. (1)) or any other model of which we are aware.

The aim of the present work was to identify differences in polymer-solution rheology ascribable to solvent/mixing procedure, polymer source and biocide. Once it became apparent that such differences were small (practically undetectable to the eye in a log–log plot such as Fig. 1) it was felt appropriate to quantify the consistency with which nominally identical fluids could be produced (i.e. using the same solvent, mixing procedure, polymer batch and biocide) and characterised. Fig. 1, therefore, includes seven sets of data: the five sets identified in Section 2 (i.e. LLXF, LPXF, PLXF, PPXF and LLXK) together with two additional sets (LLXF2 and LLXF3) for fluids nominally identical to LLXF.

We have fitted the Carreau–Yasuda model individually to each of the seven sets of data to determine the "inherent" standard deviation σ_I and the Pearson correlation coefficient R. The inherent standard deviation

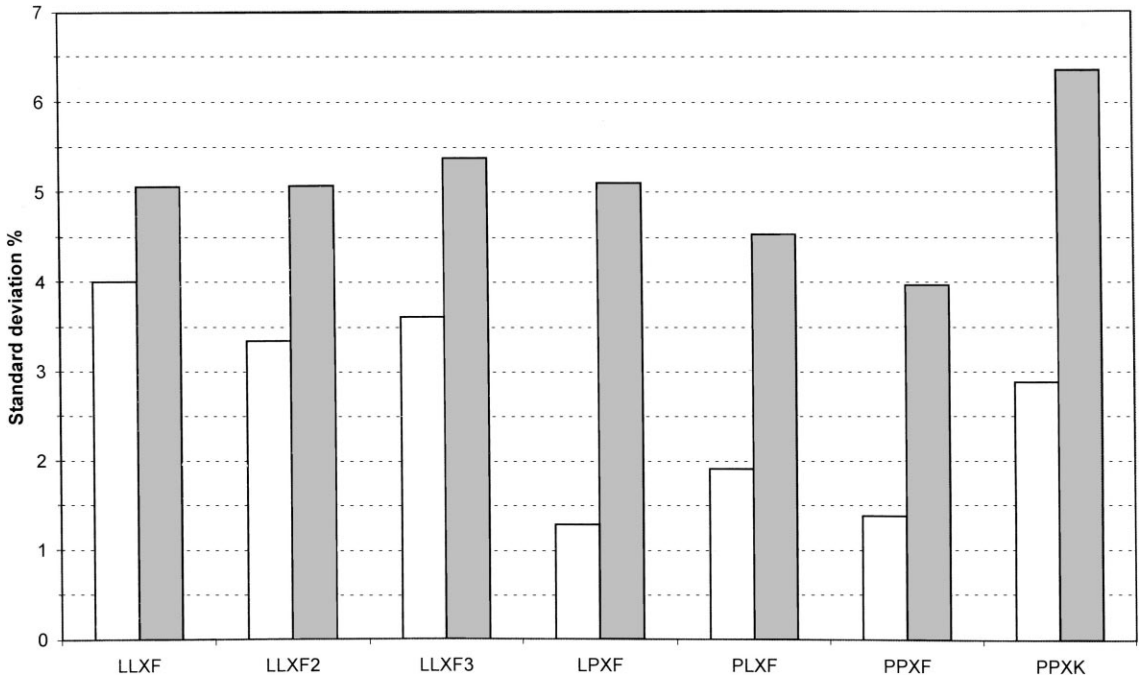

Fig. 2. Standard deviations σ_I (□) and σ_A (▭) based on the Carreau–Yasuda model for xanthan gum viscosity.

σ_I can be attributed to two sources: first measurement uncertainty, associated with the rheometer and the measurement procedure, and second the degree to which the Carreau–Yasuda (or any other model) completely characterises the viscometric viscosity of xanthan gum. For present purposes the standard deviation is defined by

$$\sigma \equiv \sqrt{\frac{\sum(1-\mu_M/\mu_{CY})^2}{N}} \tag{3}$$

and the Pearson correlation coefficient as defined by Weiss and Hassett [17] is

$$R = \frac{N\sum\mu_M\mu_{CY} - \sum\mu_M\sum\mu_{CY}}{\sqrt{\left[N\sum\mu_M^2 - \left(\sum\mu_M\right)^2\right]\left[N\sum\mu_{CY}^2 - \left(\sum\mu_{CY}\right)^2\right]}}. \tag{4}$$

According to Syed Mustapha et al. [18], a correlation is unacceptably poor for rheological work of the type under discussion if $R < 0.9975$. We have preferred to list $(1-R)$ so that acceptable correlations correspond to $(1-R) < 2.5\times10^{-3}$. As can be seen from Table 2, this criterion is well satisfied in all cases, the lowest value of R being 0.9982. Table 2 includes the model parameters for these fits, the N, σ_I and $(1-R)$ values and the ranges of $\dot{\gamma}$, τ and μ_M. Also included are values for the standard deviation σ_A for the individual data sets but for which μ_{CY} was calculated from the curve fit of the Carreau–Yasuda model to the entire data set.

The standard deviations σ_I and σ_A for XG are presented as a bar chart in Fig. 2. Immediately apparent is that the inherent standard deviation σ_I is practically the same for the three pure Liverpool fluids (LLXF,

Table 2
Carreau–Yasuda model parameters and correlation statistics

Fluid	μ_0 (Pa s)	$\mu_\infty \times 10^3$ (Pa s)	n	λ_{CY} (s)	a	$\dot{\gamma}_{MIN}$ (s^{-1})	$\dot{\gamma}_{MAX}$ (s^{-1})	τ_{MIN} (Pa)	τ_{MAX} (Pa)	$\mu_{MIN} \times 10^3$ (Pa s)	μ_{MAX} (Pa s)	N	σ_A (%)	σ_I (%)	$(1-R) \times 10^3$
LLXF	13.2	1.99	0.693	60.8	0.598	4.25×10^{-4}	2.03×10^4	5×10^{-3}	56.0	2.76	11.8	48	5.06	4.01	0.1
LLXF2	10.7	2.21	0.676	50.2	0.738	1.12×10^{-2}	6.30×10^3	0.1	27.1	4.30	8.93	16	5.07	3.34	1.2
LLXF3	8.89	2.05	0.678	36.9	0.844	1.27×10^{-2}	6.52×10^3	0.1	27.1	4.16	7.87	14	5.37	3.60	0.9
LPXF	15.3	2.37	0.699	63.0	0.461	9.39×10^{-4}	1.75×10^4	0.01	57.2	3.27	10.7	16	5.09	1.27	0.2
PLXF	13.6	1.89	0.702	51.6	0.562	9.18×10^{-4}	1.29×10^4	0.01	38.1	2.95	10.9	22	4.52	1.90	0.1
PPXF	15.8	2.12	0.717	53.5	0.457	3.40×10^{-3}	2.01×10^4	0.03	50.1	2.50	8.82	28	3.96	1.38	0.2
PPXK	13.0	2.78	0.693	64.0	0.631	9.08×10^{-4}	1.71×10^4	0.01	57.2	3.35	11.0	23	6.35	2.88	0.1
ALL XG	13.2	2.12	0.689	60.7	0.591	4.25×10^{-4}	2.03×10^4	5×10^{-3}	57.2	2.50	11.8	167	5.07	5.07	0.7
LLCF	0.454	6.89	1.350	0.000554	0.291	8.49×10^{-2}	1.11×10^4	0.03	126	11.4	0.353	35	2.09	1.57	0.3
LPCF	0.415	0.58	0.543	0.0649	0.392	8.43×10^{-2}	9.87×10^3	0.03	115	11.7	0.356	21	2.59	1.57	0.5
BOTH LC	0.436	4.54	0.802	0.00888	0.334	8.43×10^{-2}	1.11×10^4	0.03	126	11.4	0.356	56	2.29	2.29	0.5
PLCF	0.264	2.91	0.628	0.0380	0.557	3.28×10^{-1}	1.80×10^4	0.08	128	7.11	0.244	15	2.83	0.75	0.3
PPCF	0.262	2.75	0.587	0.0543	0.579	3.33×10^{-1}	1.81×10^4	0.08	143	7.91	0.240	16	1.08	1.06	0.0
PPCK	0.286	3.12	0.643	0.0349	0.453	3.40×10^{-1}	1.79×10^4	0.08	130	7.27	0.235	15	3.17	1.41	0.5
ALL PC	0.266	2.85	0.599	0.0496	0.557	3.28×10^{-1}	1.81×10^4	0.08	143	7.27	0.244	46	2.51	2.51	0.8

Table 3
Cross model parameters and correlation statistics

Fluid	μ_0 (Pa s)	$\mu_\infty \times 10^3$ (Pa s)	m	λ_{CR} (s)	N	σ_A (%)	σ_I (%)	$(1-R) \times 10^3$
LLXF	12.1	1.89	0.680	63.0	48	5.19	4.23	1.2
LLXF2	11.6	2.26	0.680	54.2	16	4.99	3.35	1.1
LLXF3	10.6	2.16	0.688	42.7	14	5.35	3.70	0.8
LPXF	12.2	2.17	0.667	72.2	16	5.29	2.72	0.8
PLXF	11.8	1.73	0.682	53.5	22	4.82	2.71	0.2
PPXF	10.7	1.91	0.681	49.3	28	4.66	3.04	0.6
PPXK	12.4	2.71	0.595	65.0	23	6.17	2.96	0.9
ALL XG	11.6	2.09	0.675	58.7	167	5.22	5.22	1.8

LLXF2, LLXF3) at around 3.7% and that σ_I for the "hybrid" Porto and Liverpool fluids (LPXF, PLXF) and also for the pure Porto fluid (PPXF) stands at around 1.5%. In all cases the σ_A values are higher by between 1 and 4%. The two fluids for which the difference between σ_I and σ_A is higher than average are LPXF and PPXK but the σ_A values are between 4 and 6%. It is clear that a low σ_I is not mirrored in a low σ_A, the parameter that better indicates the existence of a systematic difference. Since there is no clear trend to the observed differences, the overall conclusion is that no systematic effect of solvent/mixing procedure, polymer batch or biocide is discernible.

To explore further the influence of the viscosity model on σ_I and σ_A, we have carried out the same analysis as above for the Cross model:

$$\mu_{CR} = \mu_\infty + \frac{\mu_0 - \mu_\infty}{1 + (\lambda_{CR}\dot{\gamma})^m}, \tag{5}$$

with the corresponding parameters listed in Table 3. A curve representing the best fit of the Cross model to the XG data is also included in Fig. 1. Since the Cross model has only four parameters, against the five of Carreau–Yasuda, slightly higher standard deviations are expected a priori. In fact all the fits are still good with $(1-R)$ well within the acceptability criterion of Syed Mustapha et al. [18]. What is noticeable, however, is that now in the bar chart of the standard deviations (Fig. 3) the σ_I values for LLXF, LLXF2 and LLXF3 are practically the same as for the Carreau–Yasuda model but only slightly higher than the values for LPXF, PLXF, PPXF and PPXK. The σ_A values on the other hand show no systematic increase or decrease.

To further assess the fitting quality of the Carreau–Yasuda model we have plotted $\mu_M/\mu_{CY} - 1$ versus shear stress (Fig. 4) and this reveals quite clearly that there is both a random and a systematic contribution to σ_I. There is less scatter compared with the best fit Cross model (not shown here). For CMC, which we consider next, there is also a systematic trend but one which is different from that for XG. We conclude from these observations that the systematic trend is associated with the selected viscosity model representation rather than the rheometer/measurement procedure.

There is little to choose between the Carreau–Yasuda and Carreau (not shown in Fig. 1) model fits except at the lowest shear rates ($\dot{\gamma} < 10^{-2}\,s^{-1}$) where the Carreau model ($a = 2$) asymptotes to a lower value of μ_0 than the Carreau–Yasuda model. This difference is associated with the entirely different behaviour of the two models at infinitesimally low shear rates: for $a < 1$, the Carreau–Yasuda model approaches μ_0 with infinite gradient $d\mu/d\dot{\gamma}$ whereas the Carreau model exhibits a Newtonian plateau

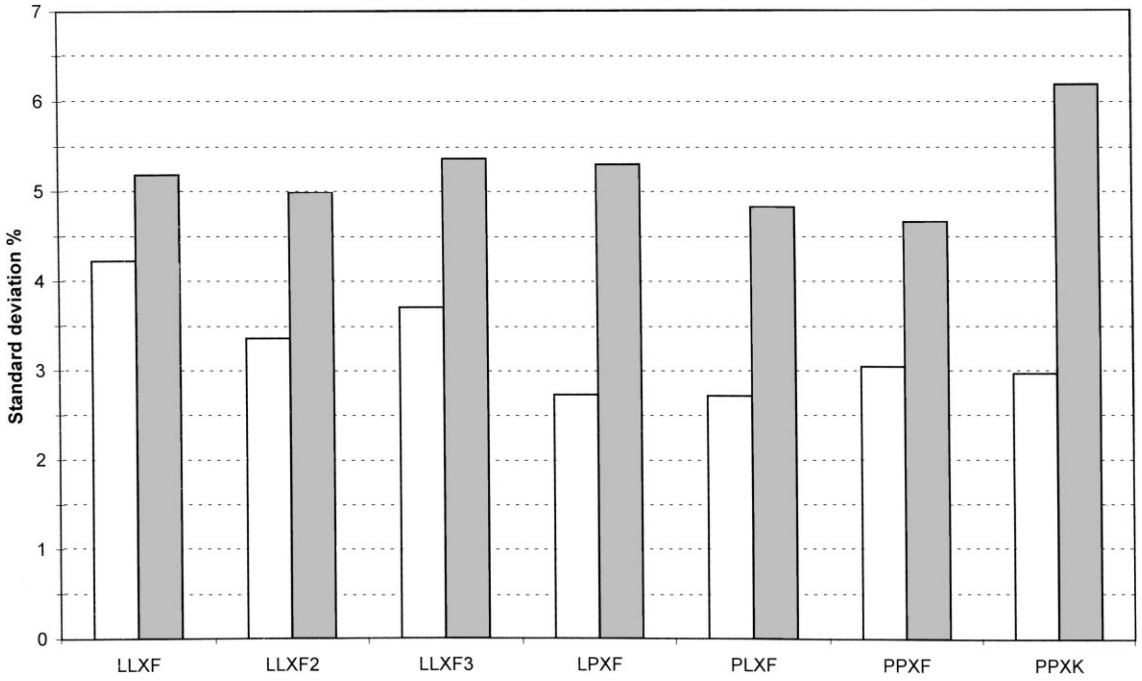

Fig. 3. Standard deviations σ_I (□) and σ_A (▭) based on Cross model for xanthan gum viscosity.

associated with zero gradient. The Cross model behaves in the same way as the Carreau–Yasuda model for $a < 1$.

4.1.2. Carboxymethylcellulose (CMC)

The CMC data plotted in Fig. 5 reveal that the Aldrich CMC used in Liverpool produces a fluid about 30% more viscous than the Porto polymer manufactured by Hercules. Here again, however, there is no discernible difference associated with the water solvent. The two sets of curves (△, ▲, + and □, ■) have qualitatively the same shear-thinning trend, suggesting that the differences are due to molecular weight, that for the BDH polymer being greater than that from Hercules.

The statistical data in Fig. 6 and Table 2, reveal that the inherent standard deviation σ_I is higher for the Aldrich polymer. In view of our conclusions for XG, it seems that the differences in molecular weight affect not only the viscosity level but also the dependence of viscosity on shear stress/shear rate. Fig. 6 also shows that for the Liverpool (Aldrich) polymer the transition from power-law behaviour to the first Newtonian plateau takes place over a wider range of shear rates than for the Porto (Hercules) polymer. This difference is reflected in the lower values of a for the Liverpool polymer and also suggests a wider distribution of molecular weight. There is some evidence for these suggestions regarding molecular weight in Fig. 7 where the LLCF data show a systematic variation not apparent in the other three data sets. Apart from this set, however, the Carreau–Yasuda model is quite clearly an excellent fit to the CMC viscosity data.

If the bar charts for the two fluids are compared, we see that the highest overall σ_A values for both CMC and XG are obtained for solutions prepared with the Porto polymers and solvent with Kathon as

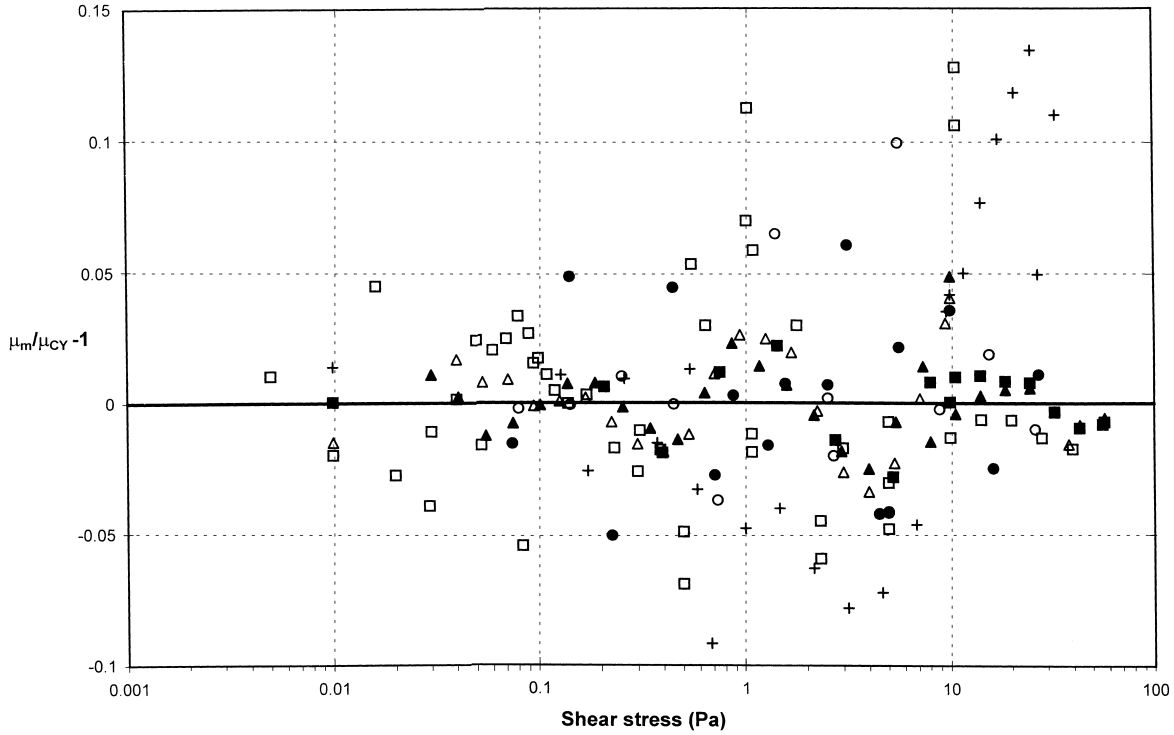

Fig. 4. Difference between experimentally determined viscosity and Carreau–Yasuda model fit for xanthan gum (symbols as for Fig. 1).

the biocide (i.e. PPCK and PPXK). Although this increase in σ_A is small, it could indicate an influence of the biocide.

The highest σ_I values are for solutions prepared with the Liverpool polymers and solvent (LLXF and LLCF), whereas for XG the lowest σ_I is for LPXF and for CMC it is PLCF, confirming that there is no consistent influence of the solvent.

The minimum shear rates obtainable for the CMC solutions plotted in Fig. 5 are noticeably greater (of the order of two orders of magnitude) than those obtained for the xanthan gum solutions. This can be attributed to CMC's lower zero shear-rate viscosity value (<3% of xanthan gum) so that when the minimum shear stress of the rheometer is applied, a much higher shear rate results for the CMC solution compared to the xanthan gum solution.

4.2. Oscillatory tests

The 6 cm diameter, 2° acrylic cone geometry was used to provide the oscillation data to minimise the effects of inertia. A linearity check was conducted for each fluid to determine the linear viscoelastic region prior to each frequency sweep. All frequency sweeps were performed at a shear stress of 0.1 Pa, a value well within the linear regime. Comparison with frequency sweep data at 1 Pa, again within the linear

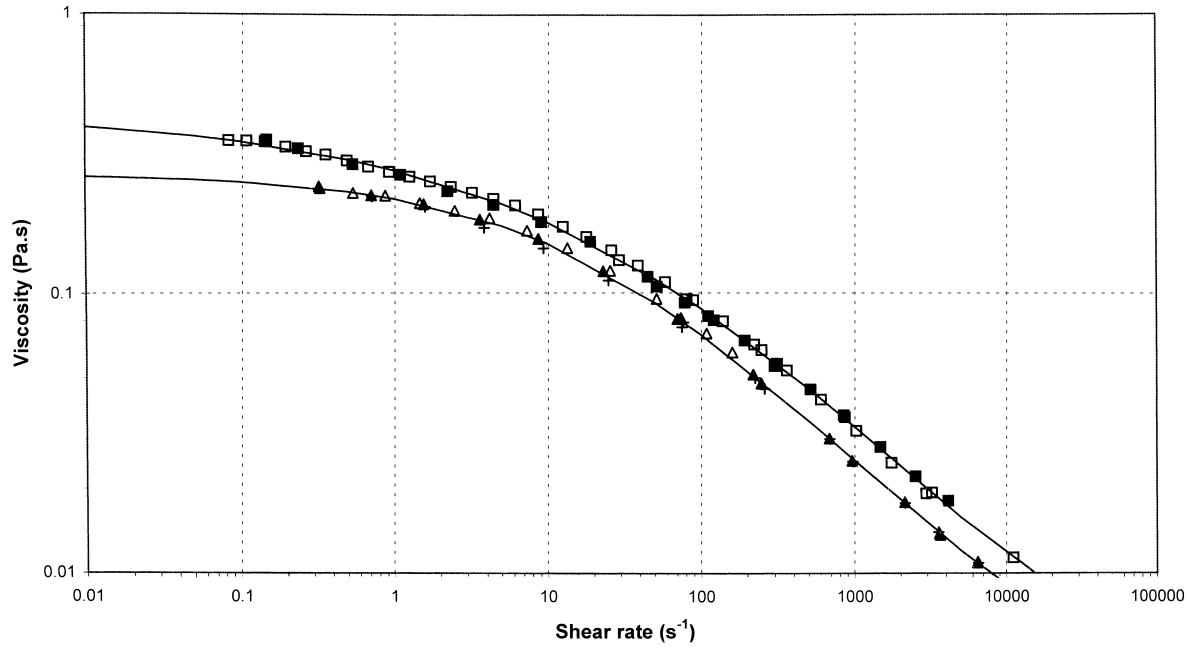

Fig. 5. Viscometric viscosity of CMC solutions together with Carreau–Yasuda model fits: (□) LLCF; (■) LPCF; (△) PLCF; (▲) PPCF; (+) PPCK.

region, showed good agreement and confirmed that the viscoelastic properties observed were independent of the shear-stress value.

The XG results for G' and G'' plotted in Figs. 8 and 9 show that there is no systematic influence on either modulus of the polymer itself or the water solvent. In Figs. 10 and 11 the storage (G') and loss

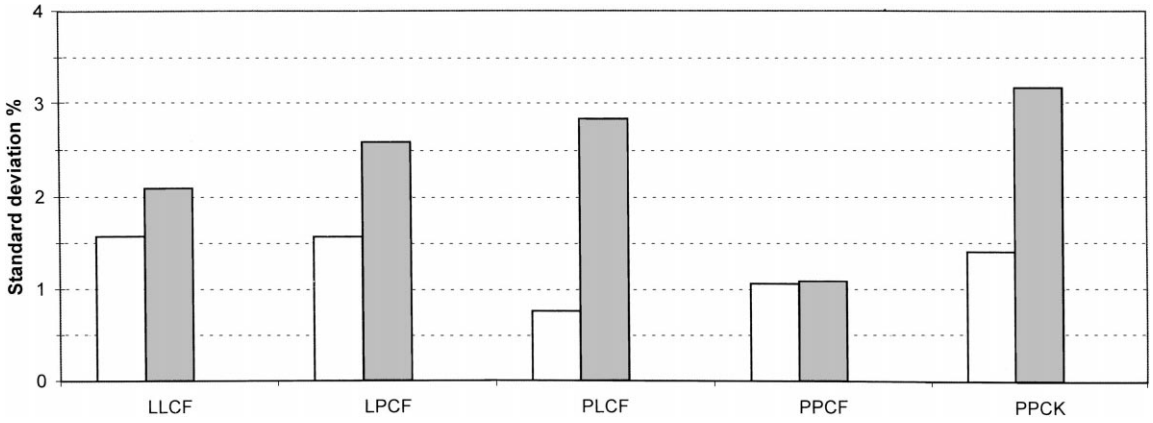

Fig. 6. Standard deviations σ_I (□) and σ_A (▭) based on Carreau–Yasuda model fit for CMC viscosity.

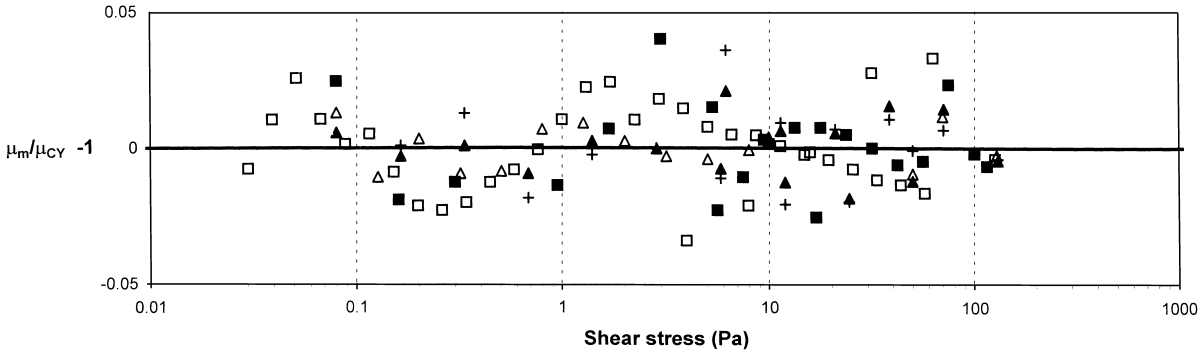

Fig. 7. Difference between experimentally determined viscosity for CMC and Carreau–Yasuda model fits (symbols as for Fig. 5).

(G'') moduli are plotted for CMC. The lower magnitude of both moduli, and particularly G', for CMC compared with those for XG leads to an increase in the scatter of the data, especially at low frequencies of oscillation. However, as a comparison between Figs. 8 and 10 shows, it is at low frequencies that the higher elasticity of the xanthan gum solutions becomes apparent, with G' for XG an order of magnitude higher at frequencies of about 10^{-2} Hz but tending to the same level as for CMC at frequencies around 10 Hz. It is remarkable that although the viscosity of the BDH CMC is 30% higher than that of the Hercules CMC there is practically no polymer effect upon G' or G''. The reason for these different behaviours is certainly related to the different molecular configurations in both flows. In the steady shear flow used in the viscosity measurements the molecules are uncoiled by the shear forces and the longer molecules result in higher

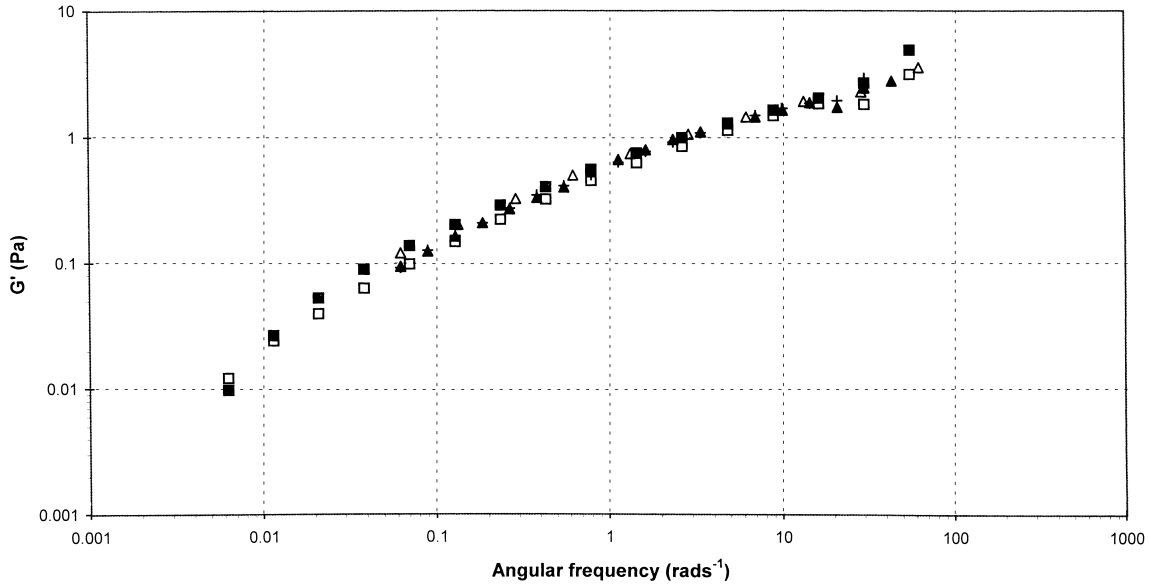

Fig. 8. Storage modulus G' of xanthan gum solutions: (□) LLXF; (■) LPXF; (△) PLXF; (▲) PPXF; (+) PPXK.

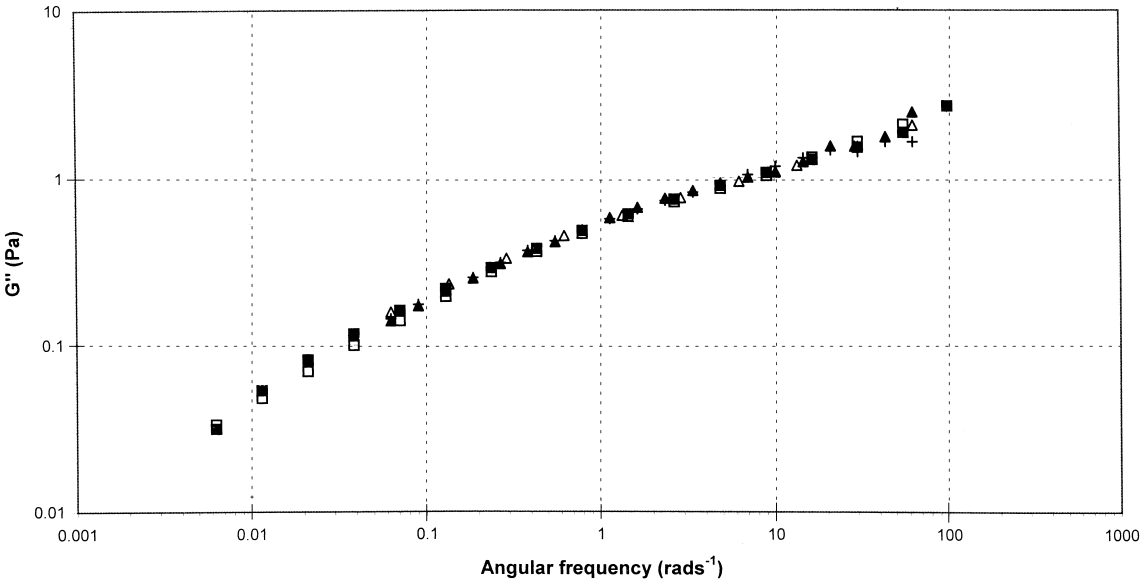

Fig. 9. Loss modulus G'' of xanthan gum solutions (symbols as for Fig. 8).

flow resistance. In oscillatory shear flow the molecules stay in the near-equilibrium configuration and the resistance is less sensitive to small differences in molecular length. However, as for XG, for neither CMC was there evidence of any influence of the solvent. The data were also compared with that from fluids prepared in the large flow loop at Liverpool, and again no significant differences were found.

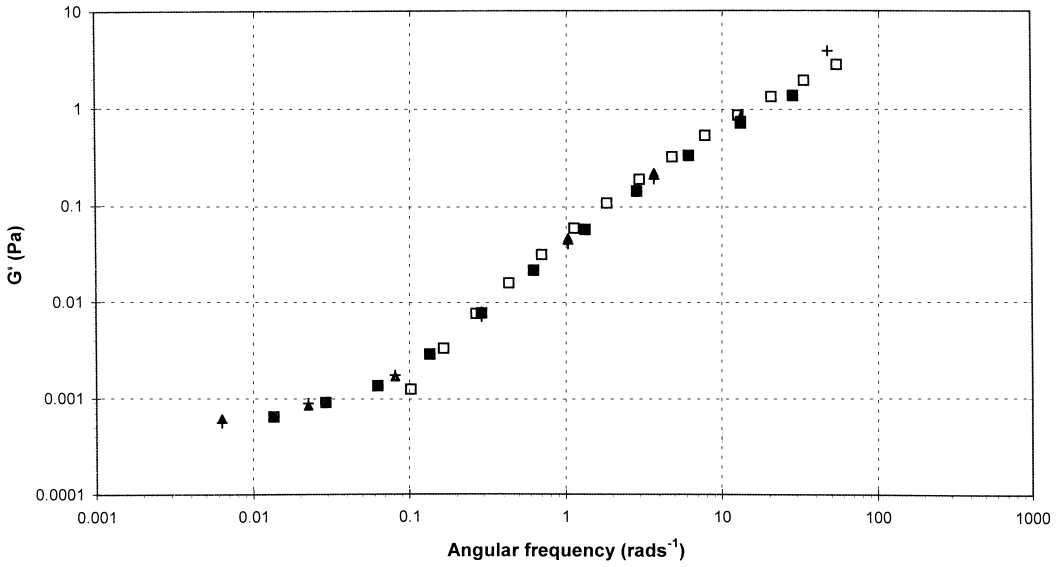

Fig. 10. Storage modulus G' of CMC solutions: (□) LLCF; (■) LPCF; (△) PLCF; (▲) PPCF; (+) PPCK.

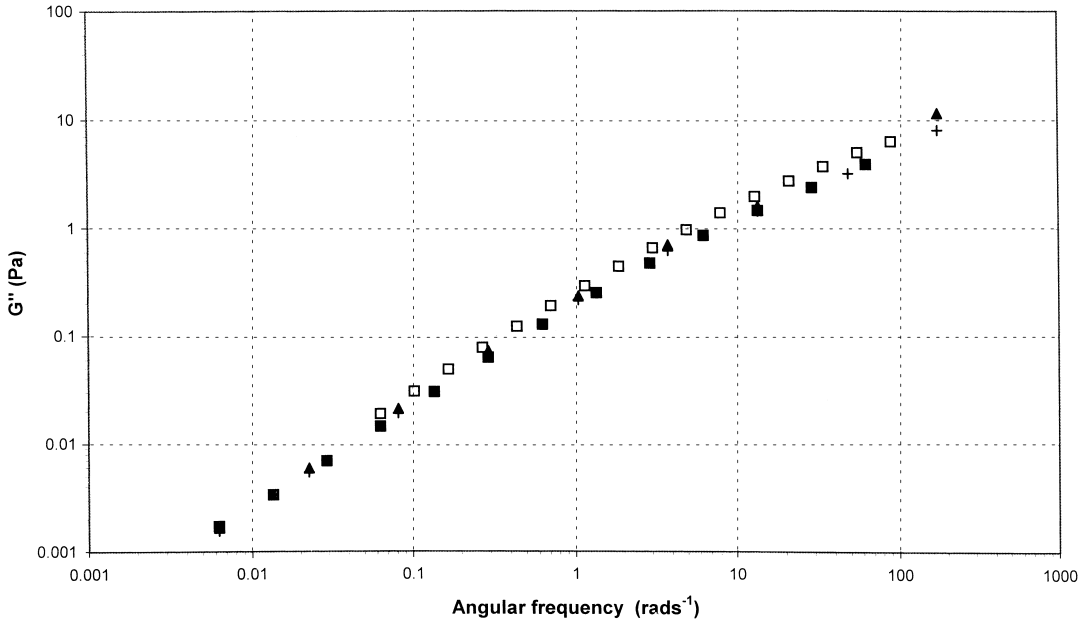

Fig. 11. Loss modulus G'' of CMC solutions (symbols as for Fig. 10).

5. Concluding remarks

The most important conclusion of this work is that for the test polymer solutions, carboxymethylcellulose and xanthan gum, there seems to be negligible influence of the tap-water solvent and method of preparation of the fluids on either the viscosity or the storage and loss moduli, thus, facilitating comparisons of hydrodynamic results from different laboratories. A very small influence could be ascribed to the biocide used but is not practically significant.

For practical purposes, the same rheology resulted for aqueous solutions of xanthan gum manufactured from polymers having the same grades and manufactured by the same company, even though almost certainly manufactured at different times.

Although the viscosities of the solutions based on the CMC supplied by BDH were 30% higher than those based on the CMC from Hercules, the differences in the loss and storage moduli were within experimental uncertainty.

As pointed out in Section 1, other polymers such as polyacrylamide and carbopol show less consistency in their rheological properties. In the absence of the collaborative arrangements we advocate, comparisons and scaling laws based upon data from different laboratories using nominally identical fluids have to be viewed with caution.

Acknowledgements

This work was facilitated by an exchange programme, jointly financed by The British Council and Junta Nacional de Investigação Cientifica e Tecnológica (JNICT), within the framework of the Treaty

of Windsor, programme number Lis/882/12 (95/96) to whom the authors are grateful. Purchase of the TA Instruments rheometer was possible thanks to EPSRC research grant GR/M91716. The authors also acknowledge the assistance of Dr. B. Costello of TA Instruments in providing information used in the uncertainty analysis of the rheometer.

Appendix A. Uncertainty analysis of the TA Rheolyst AR 1000N rheometer

A.1. Geometrical characteristics

This uncertainty analysis depends on the specific viscosity values measured with samples of aqueous solutions of 0.4% CMC and 0.25% XG. These viscosity measurements were carried out using the parallel-plate, cone-and-plate and double-concentric cylinder geometries. This analysis refers to the latter, which was the geometry used at the low end of the shear rate range where uncertainties are higher. At the end of this Appendix A we explain briefly the effect of geometry type upon the total uncertainty. The double-concentric geometry has an inner annular gap defined by $r_I = 20.00\,\text{mm}$ and $R_I = 20.38\,\text{mm}$, an outer gap based on $r_O = 21.96\,\text{mm}$ and $R_O = 22.38\,\text{mm}$, and the immersed length L of the cylinder is 20.5 mm. The radius ratio ε is 0.981 for each gap and consequently, for Couette flow of a Newtonian fluid, the fraction of the total torque measured in the inner and outer gaps can be determined as

$$\frac{M_I}{M_T} = 0.4533 \quad \text{and} \quad \frac{M_O}{M_T} = 0.5467 \tag{A.1}$$

A.2. Fluids

As shown in Section 4.1 of the main text, the viscosities of the 0.4% CMC and 0.25% XG solutions are best represented by the Carreau–Yasuda model (Eq. (1)). However, since some terms of the total uncertainty need to be quantified on the basis of the exponent n of a power-law fit, power laws were fitted to the viscosity of these solutions over various ranges of shear rate to determine values of n. The results are listed in the middle column of Tables 4 and 5.

A.3. Total uncertainty, bias and precision error limits

The uncertainty analysis follows the philosophy outlined in Coleman and Steele [19]. The total uncertainty in the viscosity measurements (U_μ) is calculated as

Table 4
Determination of the bias error associated with the Newtonian simplification for XG solutions

Range of $\dot{\gamma}$	n	$\Delta\mu/\mu$ (%)
$0.000425\,\text{s}^{-1} \le \dot{\gamma} \le 0.01\,\text{s}^{-1}$	0.854	0.02
$0.01\,\text{s}^{-1} \le \dot{\gamma} \le 1.00\,\text{s}^{-1}$	0.482	0.09
$1.00\,\text{s}^{-1} \le \dot{\gamma} \le 100\,\text{s}^{-1}$	0.342	0.11
$100\,\text{s}^{-1} \le \dot{\gamma} \le 20300\,\text{s}^{-1}$	0.538	0.08
Whole range	0.471	0.09

Table 5
Determination of the bias error associated with the Newtonian simplification for CMC solutions

Range of $\dot{\gamma}$	n	$\Delta\mu/\mu$ (%)
$0.0849\,s^{-1} \le \dot{\gamma} \le 10\,s^{-1}$	0.878	0.02
$10\,s^{-1} \le \dot{\gamma} \le 100\,s^{-1}$	0.677	0.05
$100\,s^{-1} \le \dot{\gamma} \le 11100\,s^{-1}$	0.551	0.08
Whole range	0.695	0.05

$$U_\mu = \sqrt{B_\mu^2 + P_\mu^2} \tag{A.2}$$

or in normalised form as

$$\frac{U_\mu}{\mu} = \sqrt{\left(\frac{B_\mu}{\mu}\right)^2 + \left(\frac{P_\mu}{\mu}\right)^2} \tag{A.3}$$

where B_μ and P_μ represent estimates of the bias and precision error limits. The bias is a fixed error that can be reduced by calibration, but which has not been removed either because the calibration was not performed or because those contributions were not included in the calibration. This happens whenever an estimate rather than the exact value of the bias is known. The precision error is the variable error that can be reduced statistically by the use of multiple readings. The inherent distinction between the two types of error suggests that we treat them separately until the end, where they are combined to yield the total uncertainty.

Given that the viscosity is a function of several variables

$$\mu = \mu(x_1, x_2, \ldots, x_j), \tag{A.4}$$

the sensitivity coefficients are defined by

$$\theta_i \equiv \frac{\partial \mu}{\partial x_i}. \tag{A.5}$$

Following Coleman and Steele [19], the bias limit for the viscosity is then expressed as

$$B_\mu^2 = \sum_{i=1}^{J} \left[\theta_i^2 B_i^2 + \sum_{k=1}^{J} \theta_i \theta_k \rho_{ik} B_i B_k (1 - \delta_{ik}) \right] \tag{A.6}$$

where δ_{ik} is the Kronecker delta ($\delta_{ik} = 1$ when $i = k$, but 0 otherwise) and $\rho_{ik} = \rho_{ki}$ are the coefficients of correlation between biases in x_i, and x_k. The first term on the right-hand-side calculates the individual bias contributions to the total bias assuming total independence of events whereas the second term makes the necessary corrections when the measurements of variables are not independent (for instance, the difference between measurements of two quantities using the same instrument, such as a temperature difference). The precision error limit of the viscosity is determined in a similar fashion except that there are no corrections for correlated error contributions because the precision is inherently random. Accordingly,

$$P_\mu^2 = \sum_{i=1}^{J} [\theta_i^2 P_i^2]. \tag{A.7}$$

Finally, we note that each contribution to the bias limit B_i, or precision error limit P_i, can be made up of biases or precisions from M significant elemental error sources, i.e.

$$B_i^2 = \left[\sum_{k=1}^{M}(B_i)_k^2\right] \quad \text{and} \quad P_i^2 = \left[\sum_{k=1}^{M}(P_i)_k^2\right]. \tag{A.8}$$

Here, we are concerned with the uncertainty of viscosities which vary with the shear rate, a quantity which must also be measured and its uncertainty estimated using similar equations to the above.

A.4. Equations of reduction

A.4.1. Viscometric viscosity

The viscosity depends on torque (M), angular velocity (ω) and geometry (R,L) whereas the shear rate depends only on ω, R and L. In a single gap concentric cylinder the viscosity of a Newtonian fluid is given by

$$\mu = \frac{M}{4\pi L\omega R^2}\frac{1-\varepsilon^2}{\varepsilon^2} \tag{A.9}$$

where R now represents the outer radius. In the case of a double-gap geometry both annuli contribute to the total torque, so generally we can say that

$$\mu = \frac{M_\mathrm{I}}{4\pi L\omega R_\mathrm{I}^2}\frac{1-\varepsilon_\mathrm{I}^2}{\varepsilon_\mathrm{I}^2} \quad \text{and} \quad \mu = \frac{M_\mathrm{O}}{4\pi L\omega R_\mathrm{O}^2}\frac{1-\varepsilon_\mathrm{O}^2}{\varepsilon_\mathrm{O}^2} \tag{A.10}$$

with the subscripts I and O indicating inner and outer gap, respectively. Note that R_I, and R_O are the outer radii in each gap. Eq. (A.10) pertain to Newtonian fluids, the assumption upon which most rheometer manufacturers base their software although for a non-Newtonian fluid this leads to a bias error that will be quantified later.

The total torque is the sum of the torques in the two gaps, i.e.

$$M = 4\pi L\omega\mu\left[R_\mathrm{I}^2\frac{\varepsilon_\mathrm{I}^2}{1-\varepsilon_\mathrm{I}^2} + R_\mathrm{O}^2\frac{\varepsilon_\mathrm{O}^2}{1-\varepsilon_\mathrm{O}^2}\right] \tag{A.11}$$

so that

$$\mu = \frac{M}{4\pi L\omega[R_\mathrm{I}^2(\varepsilon_\mathrm{I}^2/(1-\varepsilon_\mathrm{I}^2)) + R_\mathrm{O}^2(\varepsilon_\mathrm{O}^2/(1-\varepsilon_\mathrm{O}^2))]}. \tag{A.12}$$

Although $\varepsilon_\mathrm{I} = \varepsilon_\mathrm{O}$, ε_I and ε_O are intentionally retained since there are contributions to the total uncertainty coming from the uncertainties in the individual measurements of the four different radii of the double gap.

A.4.2. Shear rate

The shear rate depends on angular velocity and geometry with the added complication that it is not constant across each gap and different shear rates exist in both gaps, i.e.

$$\dot\gamma_\mathrm{I} = \frac{2\omega\varepsilon_\mathrm{I}^2}{1-\varepsilon_\mathrm{I}^2} \quad \text{and} \quad \dot\gamma_\mathrm{O} = \frac{2\omega}{1-\varepsilon_\mathrm{O}^2} \tag{A.13}$$

so that even though $\varepsilon_I = \varepsilon_O$ (=0.981 here) the shear rates are different. The two shear rates are at the bob surface, which is directly connected to the torquemeter and the angular displacement transducer.

A.5. Contributions to the total uncertainty of viscosity and shear rate

The total uncertainty can be calculated from Eq. (A.3) provided B_μ and P_μ are known. These quantities are determined from the elemental sources using Eqs. (A.6) and (A.7), respectively.

A.5.1. Bias error limit of the viscosity

The relative bias error of the viscosity is given by

$$\left(\frac{B_\mu}{\mu}\right)^2 = \left(\frac{B_M}{M}\right)^2 + \left(\frac{B_\omega}{\omega}\right)^2 + \left[2\frac{B_{R_O}}{R_O}\frac{\varepsilon^2}{1-\varepsilon^2}\right]^2 + \left[-2\frac{B_{R_I}}{R_I}\frac{\varepsilon^2}{1-\varepsilon^2}\right]^2 - 8\frac{B_{R_O}}{R_O}\frac{\varepsilon^2}{1-\varepsilon^2}\frac{B_{R_I}}{R_I}\frac{1}{1-\varepsilon^2}. \tag{A.14}$$

A.5.2. Bias error limit of the shear rate

From Eq. (A.13) combined with Eq. (A.6), the bias error limit for the shear rate is given by

$$\left(\frac{B_{\dot\gamma}}{\dot\gamma}\right)^2 = \left(\frac{B_\omega}{\omega}\right)^2 + \left[2\frac{B_{R_O}}{R_O}\frac{\varepsilon^2}{\varepsilon^2-1}\right]^2 + \left[2\frac{B_{R_I}}{R_I}\frac{\varepsilon^2}{\varepsilon^2-1}\right]^2 - 8\frac{B_{R_O}}{R_O}\frac{B_{R_I}}{R_I}\left[\frac{\varepsilon^2}{\varepsilon^2-1}\right]^2 \tag{A.15}$$

which, with $B_{R_O} = B_{R_I} = B_R$, simplifies to

$$\left(\frac{B_{\dot\gamma}}{\dot\gamma}\right)^2 = \left(\frac{B_\omega}{\omega}\right)^2 + 4\left[\frac{\varepsilon^2}{\varepsilon^2-1}\right]^2 B_R^2\left[\frac{1}{R_O^2} + \frac{1}{R_I^2} - \frac{2}{R_O R_I}\right]. \tag{A.16}$$

A.5.3. Precision error limit of the viscosity

The combination of Eqs. (A.7) and (A.12) produces the precision error limit of the viscosity

$$\left(\frac{P_\mu}{\mu}\right)^2 = \left(\frac{P_M}{M}\right)^2 + \left(\frac{P_\omega}{\omega}\right)^2 + \left[2\frac{P_{R_O}}{R_O}\frac{\varepsilon^2}{1-\varepsilon^2}\right]^2 + \left[-2\frac{P_{R_I}}{R_I}\frac{1}{1-\varepsilon^2}\right]^2, \tag{A.17}$$

i.e. the difference compared with the corresponding bias error equation (Eq. (A.10)) is that now there is no correlated measurement contribution.

A.5.4. Precision error limit of the shear rate

For the precision error limit of the shear rate, Eqs. (A.7) and (A.13) combine to yield

$$\left(\frac{P_{\dot\gamma}}{\dot\gamma}\right)^2 = \left(\frac{P_\omega}{\omega}\right)^2 + \left[2\frac{P_{R_O}}{R_O}\frac{\varepsilon^2}{\varepsilon^2-1}\right]^2 + \left[2\frac{P_{R_I}}{R_I}\frac{\varepsilon^2}{\varepsilon^2-1}\right]^2. \tag{A.18}$$

A.6. Quantification of the bias

The general sources of bias identified in Section A.5 are those originating in the measurements of torque, angular velocity and radius. Other sources of bias exist but can be regarded as elemental contributions to the general sources mentioned above. This is the case, for instance, of temperature.

Table 6
Torquemeter calibration check

Set torque (μN m)	Percentage difference (%)
1991	−0.43
3002	0.06
3993	−0.18
5003	0.06
6033	0.55
7029	0.41
8020	0.25
9030	0.33

A.6.1. Temperature variation and control

The temperature control of the samples is carried out within ±0.1°C, according to the manufacturer (Costello [20]). All the measurements were carried out at a temperature of 25°C from which the room temperature does not differ by more than 5°C. Thus, we estimate the variation of the temperature across the annular gap to be well less than 0.1°C and, accordingly, only the control variation is taken into account. The uncertainty of temperature variation affects the viscosity of the solutions which has an effect upon the measurement of the torque because of the dependence of fluid viscosity on temperature. For small temperature differences the viscosity can be assumed to vary linearly with temperature in a similar way to that of water (3%/°C). From the linear relationship between torque and viscosity (Eq. (A.12)), the temperature control accuracy will have a relative contribution to the total torque bias $B_{1_M}/M = 0.3\%$.

A.6.2. Torquemeter bias

For the torquemeter, it is necessary to distinguish between high and low values of torque. In the upper range, we have quantified the bias on the basis of the calibration provided by the manufacturer and presented in Table 6. These differences were not used to correct readings and consequently are estimates of the bias limit in the torquemeter reading.

As can be seen, the differences between imposed and measured torque vary between −0.43 and 0.55%, with more positive than negative values. We have opted for the largest value and assumed it to apply in the torque range above 2000 μN m, so that the estimate of the bias in the torquemeter is $B_{2_M}/M = \pm 0.55\%$.

In the low torque region the bias limit is likely to be larger. According to the manufacturer (Costello [20]), in the range 10–1000 μN m the torque should be within ±1% at zero speed, with a small correction to this value if the speed is non-zero. However, provided the speed is less than 1 rad/s, this error will be negligible. A further correction is introduced to allow for bearing runout in the bearing mapping and so a further 0.1 μN m should be allowed for bias. Finally, there will also be residual friction in the bearing (besides the runout) which can be removed by calibrating in air and introducing the correction manually. If this is not done then at 1 rad/s an extra bias of 0.5 μN m should be added. This correction is done automatically by the software when the rheometer operates in rotating flow, but not in creep mode. Since the low shear rate measurements reported here were carried out using the creep mode, this bias source must be taken into account. With this limited amount of information these values will be generalised and assumed to apply to the whole low range of torque. This is a conservative estimate for higher rotational speeds but may result in underestimation at very low rotational speeds.

Table 7
Typical measured values for 0.25% XG

$\dot{\gamma}$ (s^{-1})	μ (Pa s)	ω (rad/s)	M (μN m)	B_{2_M}/M (%) (creep)	B_{2_M}/M (%) (no creep)
0.0005	11.048	9.6190e^{-6}	0.65184	78.2	15.4
0.001	10.498	1.9238e^{-5}	1.2388	41.2	8.1
0.005	8.3117	9.6190e^{-5}	4.9040	10.5	2.3
0.01	6.9935	0.00019238	8.2525	6.3	1.6
0.05	3.8040	0.00096190	22.444	2.5	1.1
0.1	2.6928	0.0019238	31.776	1.9	1.0
0.5	1.0591	0.0096190	62.487	1.3	1.0
1	0.68415	0.019238	80.732	1.3	1.0
5	0.23916	0.096190	141.11	1.1	1.0
10	0.15108	0.19238	178.28	1.0	1.0
50	0.052236	0.96190	308.20	1.0	1.0
100	0.033360	1.9238	393.66	1.0	1.0
500	0.012436	9.6190	733.72	1.0	1.0
1000	0.0084707	19.238	999.56	1.0	1.0
5000	0.0040869	96.190	2411.3	0.55	0.55

As a result of these various contributions, at low torque we have the following relative bias limit

$$\frac{B_{2_M}}{M} = \sqrt{0.01^2 + \left(\frac{0.1}{M}\right)^2 + \text{creep} \times \left(\frac{0.5}{M}\right)^2} \tag{A.19}$$

where "creep" takes the value 1 for a creep test and 0 otherwise (note that M is in μN m).

Since the relative uncertainty is no longer constant, but depends on the value of torque, it is necessary to know representative values of torque and in Tables 7 and 8 such information is summarised for the low torque region.

A.6.3. Accuracy of geometrical dimensions

According to Costello [20], the measurements of the diameters are accurate to within ± 0.025 mm. As this is a very sensitive part of the rheometer, and can lead to very large errors, a special measuring device was used by the manufacturer to carry out the measurements of diameters, all four being measured

Table 8
Typical measured values for 0.4% CMC

$\dot{\gamma}$ (s^{-1})	μ (Pa s)	ω (rad/s)	M (μN m)	B_{2_M}/M (%) creep	B_{2_M}/M (%) no creep
0.1	0.33872	0.0019238	3.9970	12.8	2.7
0.5	0.30630	0.0096190	18.072	3.0	1.1
1	0.28551	0.019238	33.690	1.8	1.0
5	0.22106	0.096190	130.43	1.1	1.0
10	0.18869	0.19238	222.66	1.0	1.0
50	0.11598	0.96190	684.30	1.0	1.0
100	0.089791	1.9238	1059.6	1.0	1.0
500	0.045860	9.6190	2705.8	0.55	0.55

with the same instrument. This is a very important consideration and only in this way is it possible to remove/decrease the amount of total bias that could be introduced by the geometrical measurements. Consequently $B_R = B_{R_O} = B_{R_I} = 0.025\,\text{mm}$.

A.6.4. Accuracy of the motor drive

Based upon information from the manufacturer that the motor drive has been calibrated to a tolerance of ±1.5% at a fixed torque of 5000 μN m referenced to a standard weight, this calibration accuracy will be applied to all measurements.

A.6.5. Newtonian simplification

In Section A.4 it was mentioned that rheometer manufacturers usually calculate the viscosity assuming the fluid inside the annulus behaves as a constant viscosity fluid, whereas in general this is obviously not the case. The errors incurred in such an approach are small unless the gap is wide. Even for a wide gap, the range of shear rates from the inner to the outer surface of the gap is still sufficiently small that a power-law description can be assumed to prevail across it, even if the flow curve as a whole shows the fluid to behave differently. Based on this assumption it is possible to calculate the error between the true viscosity and that given by the assumed constant viscosity equations. From the values of the power-law exponent in Tables 4 and 5, the resulting bias in viscosity is tabulated in column 3 of these two tables for XG and CMC, respectively. All values are positive, but for the sake of simplicity in the ensuing analysis they will be considered as ± values.

Although the Newtonian simplification also results in a bias of the shear rate, the shear rate bias and the true viscosity bias can be combined into a single equivalent viscosity bias. Since the viscosity reduction equation in Section A.4 is not yet combined with the shear rate bias to give the equivalent viscosity bias, this contribution to the total uncertainty must be added at the end, after determination of the equivalent bias. This effect is in any case rather small and can be simply quantified as ±0.1% for the XG solution and ±0.05% for the CMC solution.

A.7. Quantification of the sources of precision error limit

Basically, all the measurements referred to previously are also sources of precision error. The precision errors of those measurements are related to the sampling process of the reading instrument and the accuracy of the data acquisition system: the larger the sample size the smaller the precision error. According to the manufacturer of the rheometer the samples were sufficiently large that corresponding precision errors are well below the accuracy of the sensors (bias error) and in consequence negligible precision errors were assumed for all quantities.

A.8. Determination of total uncertainty

A.8.1. Total bias error

To determine the total bias error given in Eq. (A.14), the total torquemeter bias must be calculated. For high values of torque this contribution is given by

$$\left(\frac{B_M}{M}\right) = \sqrt{\left(\frac{B_{1_M}}{M}\right)^2 + \left(\frac{B_{2_M}}{M}\right)^2} = \sqrt{0.3^2 + 0.55^2} = 0.626\% \tag{A.20}$$

Table 9
Total viscosity bias in the low torque region for 0.25% XG solution

$\dot{\gamma}$ (s^{-1})	B_μ/μ (%) creep	B_μ/μ (%) no creep
0.0005	78.2	15.5
0.001	41.2	8.3
0.005	10.6	2.9
0.01	6.5	2.4
0.05	3.0	2.0
0.1	2.6	2.0
0.5	2.2	2.0
1	2.1	2.0
5	2.0	2.0
10	2.0	2.0
50	2.0	2.0
100	2.0	2.0
500	2.0	2.0
1000	2.0	2.0
5000	1.81	1.81

which after substitution in Eq. (A.14) gives

$$\left(\frac{B_\mu}{\mu}\right)^2 = \left(\frac{0.626}{100}\right)^2 + (0.015)^2 + \left[2\frac{0.025}{22.32}\frac{0.981}{(1-0.981)^2}\right]^2 + \left[-2\frac{0.025}{20.38}\frac{1}{(1-0.981)^2}\right]^2 - 8\frac{0.025}{22.32}\frac{0.981^2}{(1-0.981)^2}\frac{0.025}{20.38}\frac{1}{(1-0.981)^2} = (0.00626)^2 + (0.015)^2 + 0.0000625, \tag{A.21}$$

i.e. a final value of 1.81% is calculated regardless of the fluid because of the dominant contribution from the angular speed bias. For low values of torque the total torquemeter bias given by

$$\left(\frac{B_M}{M}\right) = \sqrt{\left(\frac{B_{1_M}}{M}\right)^2 + \left(\frac{B_{2_M}}{M}\right)^2} = \sqrt{0.3^2 + \left(\frac{B_{2_M}}{M}\right)^2} \tag{A.22}$$

where B_{2_M}/M is given by Eq. (A.19) and is tabulated in Tables 7 and 8 for XG and CMC, respectively, depending on whether the viscosity measurements were performed in creep or rotational mode. Eq. (A.22) is inserted into Eq. (A.14) for the total bias in viscosity which becomes

$$\left(\frac{B_\mu}{\mu}\right)^2 = \left(\frac{B_M}{M}\right)^2 + (0.015)^2 + \left[2\frac{0.025}{22.32}\frac{0.981^2}{(1-0.981)^2}\right]^2 + \left[-2\frac{0.025}{20.38}\frac{1}{(1-0.981)^2}\right]^2 - 8\frac{0.025}{22.32}\frac{0.981^2}{(1-0.981)^2}\frac{0.025}{20.38}\frac{1}{(1-0.981)^2} = \left(\frac{B_M}{M}\right)^2 + (0.015)^2 + 0.0000625. \tag{A.23}$$

The total viscosity bias now depends on the shear rate and the results are tabulated in Tables 9 and 10 for the XG and CMC solutions, respectively.

Table 10
Total viscosity bias in the low torque region for 0.4% CMC

$\dot{\gamma}$ (s^{-1})	B_μ/μ (%) creep	B_μ/μ (%) no creep
0.1	12.9	3.2
0.5	3.5	2.0
1	2.5	2.0
5	2.0	2.0
10	2.0	2.0
50	2.0	2.0
100	2.0	2.0
500	1.81	1.81

The bias from the torquemeter is high at very low shear rates, and so dominates the total viscosity bias, but at higher values of torque the contributions from the torque and the rotational speed measurements are both important and a total bias of about 2% is approached.

A.8.2. Total precision error limit

Since the precision error limits were considered negligible in comparison with the bias limit, they are taken as zero. Therefore, the total viscosity uncertainty equals the total bias in viscosity, i.e. 1.81% at high torque and the values in Tables 9 and 10 in the low torque range.

A.8.3. Bias and precision error limits of the shear rate

For the shear rate the bias error contributions are combined as follows:

$$\frac{B_{\dot{\gamma}}}{\dot{\gamma}} = (0.015)^2 + 4\left[\frac{\varepsilon^2}{\varepsilon^2 - 1}\right]^2 (0.025)^2 \times [7.3 \times 10^{-7}] = (0.015)^2 + 1.22 \times 10^{-6} \tag{A.24}$$

and it is seen that the total bias error for shear rate is basically that of the angular speed and equal to 1.5%.

A.9. Equivalent viscosity uncertainty

So far we have total uncertainties for viscosity (U_μ/μ) and for shear rate ($U_{\dot{\gamma}}/\dot{\gamma}$) and also an equivalent bias error for viscosity originating from the Newtonian behaviour assumption ($U_{\mu,\text{Newtonian}} = B_{\mu,\text{Newtonian}}$). Since the viscosity depends on shear rate it is possible, and more convenient, to calculate an equivalent viscosity uncertainty that combines the original viscosity and shear rate uncertainties, as well as $U_{\mu,\text{Newtonian}}$. This is done here, and it is necessary to consider the different ranges of shear rate in Tables 4 and 5 because of the different power-law exponents. The equivalent viscosity uncertainty is defined as

$$\left(\frac{U_{\text{eq},\mu}}{\mu}\right)^2 = \left(\frac{U_\mu}{\mu}\right)^2 + (n-1)^2\left(\frac{U_{\dot{\gamma}}}{\dot{\gamma}}\right)^2 + \left(\frac{U_{\mu,\text{Newtonian}}}{\mu}\right)^2. \tag{A.25}$$

The effect of n and of the "Newtonian" contribution on the equivalent viscosity is assessed in Table 11 which compares $U_{\text{eq},\mu}/\mu$ with U_μ/μ for the high torque range. In the low torque range these contributions are negligible in comparison to U_μ/μ.

Table 11
The effect of n on $U_{\mathrm{eq},\mu}/\mu$ and comparison with U_μ/μ

n	U_μ/μ (%)	$U_{\mathrm{eq},\mu}/\mu$ (%)
1	1.81	1.81
0.8	1.81	1.83
0.6	1.81	1.91
0.4	1.81	2.02

Table 11 shows that for a Newtonian fluid there is little difference between $U_{\mathrm{eq},\mu}/\mu$ and U_μ/μ. The fluids tend to exhibit a Newtonian behaviour at low shear rates where the torques are small. So, in this region we can take the values of Tables 9 and 10 to represent the final equivalent viscosity uncertainty. At the high end of the low torque range $U_\mu/\mu \approx 2\%$ and this leads to $U_{\mathrm{eq},\mu}/\mu \approx 2\%$. In the other extreme of the high torque range the fluids tend to behave as pure power-law fluids having a power-law exponent in the range 0.4–0.6 and so $U_{\mathrm{eq},\mu}/\mu$ can be taken as $\approx$2%.

Finally, a comment is required regarding rheometer geometry. This analysis was carried out for the double-concentric cylinder but is equally valid for the cone-plate and parallel plate geometries because the dominant contributions to the total uncertainty are associated with the torque and the angular speed measurements provided the dependence of viscosity on torque and speed for these geometries is also linear (or inversely linear), which is indeed the case.

References

[1] J.W. Hoyt, Negative roughness and polymer drag reduction, Expt. Fluids 11 (1991) 142.
[2] M. Ollis, The scaling of drag reducing turbulent pipe flow, Ph.D. Thesis, University of Bristol, 1981.
[3] J. De Loof, B. de Lagarde, M. Petry, A. Simon, Pressure drop reduction in large industrial ducts by macromolecular additives. Part 1: Polymer efficiency, in: Proceedings of the 2nd International Conference on Drag Reduction, B2-13-36, 1977.
[4] C.B. Wang, Pipe flow of dilute polymer solutions, Ph.D. Thesis, University of Wisconsin, USA, 1969.
[5] J.J. Allan, C.A. Greated, W.D. McComb, Laser–Doppler anemometer measurements of turbulent structure in non-Newtonian fluids, J. Phys. D: Appl. Phys. 17 (1984) 533.
[6] T.S. Luchik, W.G. Tiederman, Turbulent structure in low concentration drag-reducing channel flows, J. Fluid Mech. 190 (1988) 241.
[7] J.P. Hartnett, Viscoelastic fluids: a new challenge in heat transfer, ASME J. Heat Transfer 114 (1992) 296.
[8] M.M. Reischman, W.G. Tiederman, Laser–Doppler anemometer measurements in drag-reducing channel flows, J. Fluid Mech. 70 (1975) 369.
[9] W.G. Tiederman, T.S. Luchik, D.G. Bogard, Wall-layer structure and drag reduction, J. Fluid Mech. 156 (1985) 419.
[10] M.P. Escudier, I.W. Gouldson, D.M. Jones, Flow of shear-thinning fluids in a concentric annulus, Expt. Fluids 18 (1995) 225.
[11] J.M. Nouri, H. Umur, J.H. Whitelaw, Flow of Newtonian and non-Newtonian fluids in concentric and eccentric annuli, J. Fluid Mech. 253 (1993) 617.
[12] JNNFM, J. Non-Newtonian Fluid Mech. 35 (2 + 3) (1990) 85 (Special Issue).
[13] N.E. Hudson, J. Jones, The Al project — an overview, J. Non-Newtonian Fluid Mech. 46 (1993) 69.
[14] A.S. Pereira, F.T. Pinho, Turbulent pipe flow characteristics of low molecular weight polymer solutions, J. Non-Newtonian Fluid Mech. 55 (1994) 321.
[15] P.M. Coelho, F.T. Pinho, A.R. Rodrigues, The flow of shear-thinning liquids around a cylinder: vortex shedding and drag characteristics, in: Proceedings of the 8th International Symposium on Application of Laser Techniques to Fluid Mechanics, Paper 35.3, 1996.

[16] K. Yasuda, R.C. Armstrong, R.E. Cohen, Shear flow properties of concentrated solutions of linear and star branched polystyrenes, Rheol. Acta 20 (1981) 163.
[17] N.A. Weiss, M.J. Hassett, Introductory Statistics, Addison Wesley, New York, 1991.
[18] S.M.F.D. Syed Mustapha, T.N. Phillips, C.J. Price, L.G. Moseley, T.E.R. Jones, Viscometric flow interpretation using qualitative and quantitative techniques, Eng. Appl. Art. Intell. 12 (1999) 255.
[19] H.W. Coleman, W.G. Steele Jr., Experimentation and Uncertainty Analysis for Engineers, Wiley, New York, 1989.
[20] B. Costello, Private communication, TA Europe, 2000.